Journal of Alloys and Compounds 509 (2011) 7473–7477

Contents lists available at ScienceDirect

Journal of Alloys and Compounds

journal homepage: www.elsevier.com/locate/jallcom

Structure and properties of nanostructured A357 alloy produced by melt spinning compared with direct chill ingot

Zhongwei Chen*, Yimin Lei, Haifang Zhang

State Key Laboratory of Solidification Processing, Northwestern Polytechnical University, Xi'an 710072, Shaanxi, PR China

ARTICLE INFO

Article history:
Received 29 December 2009
Received in revised form 13 April 2011
Accepted 15 April 2011
Available online 23 April 2011

Keywords:
Melt-spinning
A357 alloy
Rapid solidification
Nanostructure

ABSTRACT

The properties of nanostructured A357 ribbons produced by melt spinning were investigated using field emission gun scanning electron microscope, X-ray diffraction pattern, differential scanning calorimetry and microhardness testing in comparison with those fabricated by direct-chill (DC) casting. The solidification time and cooling rate of 46 μm thick melt-spun ribbon were estimated to be 9.13×10^{-6} s and 1.17×10^{7} K s^{-1}, respectively. The results show that the nanostructure of A357 ribbons exhibits the enhanced solid-solubility of Si in Al matrix to 2.00 wt.% and the existence of ultra-fine and homogenous dendritic structure having a dendrite arm spacing of about 200 nm. The nano-sized spherical eutectic Si crystals having a size of 50 nm were also observed. All these structural factors increase the microhardness of the ribbon which is twice as high as that of DC casting.

1. Introduction

For the fabrication of metallic alloys, rapid solidification process shows a marked enhancement of mechanical properties over the conventionally processed alloys of the same composition through the extension of solid solubility limit, the refinement of microstructure and the dispersion of secondary phases [1,2]. Furthermore, it is possible to produce metastable materials such as quasi-crystals, nano-crystals and amorphous alloys by cooling metallic melts at cooling rates exceeding 10^4 K s^{-1} [3–5]. Rapid solidification is particularly attractive for aluminum alloys because the limited equilibrium solid solubility of some alloying elements in the aluminum lattice can be extended during the rapid solidification process [6]. Due to the unique properties of Al–Si alloys and their wide applications in aerospace, automotive and electrical applications, much work has been performed to study the effect of rapid solidification on the microstructure and properties of this family of aluminum alloys.

Amongst various rapid solidification methods, besides gas atomization [2,5] and spray deposition [7], melt spinning has extensively been used. Karaköse and Keskin [8] studied the effect of solidification rate on the microstructure and microhardness of melt-spun Al–8Si–1Sb ribbon. Their results show that a solid solubility extension of 3.83 at.% Si in Al matrix and a fine and homogeneous distribution of phases are determined for the ribbon with a hardness of about 2.7 times than that of the conventionally cast alloy. Salehi et al. [9,10] reported the existence of ultra-fine and homogenous dendritic structure in the melt-spun A413.1 and Al6061 ribbons causing a hardness increase by twice as much as that of the direct-chill (DC) cast ones. The fine equiaxed cells grains with sizes in the range of 0.4–0.7 μm were observed in melt-spun A359 ribbon, and the improvement in hardness and tensile properties are related to supersaturated α-Al solid solution and the structural refinement [11]. The microstructure of a rapidly solidified Al–12 wt.% Si ribbon shows a featureless zone along the wheel-side of the ribbon besides a cellular structure and 0.5 wt.% Sb addition refines the microstructure whereas 1.0 wt.% Sb addition lead to the formation of coarse Si particles [12,13].

In addition, as far as we know in the melt-spun A357 alloy ribbon, little detailed information about the microstructure and properties is available in the present literature, even though there were some investigations on the melt-spun Al–Si alloy ribbons. In this investigation, therefore, the nanostructure and properties of melt-spun A357 ribbons were studied and compared with the conventional DC cast ingot.

2. Experimental procedures

In this study, the feedstock A357 alloy was produced by DC casting with a composition as given in Table 1. And then, the feedstock A357 alloy was melt-spun to ribbons using single roller melt-spinning as shown in Fig. 1. The polished copper wheel had a diameter of 28 cm. The rotating speed was 20 m s^{-1}. The resultant ribbons were typically about 5 mm wide and 46 μm thick.

The melt-spun A357 ribbons were characterized by using field emission gun scanning electron microscopy (FEGSEM), X-ray diffraction pattern (XRD) and differential scanning calorimetry (DSC). FEGSEM investigations were carried using SUPRA55-ZEISS operated by InLens detector at a voltage of 15 kV. The surface of the as-quenched ribbons was observed directly by FEGSEM. The XRD measurements

* Corresponding author. Tel.: +86 029 88493450 8001.
E-mail address: chzw@nwpu.edu.cn (Z. Chen).

0925-8388/$ – see front matter © 2011 Elsevier B.V. All rights reserved.
doi:10.1016/j.jallcom.2011.04.082

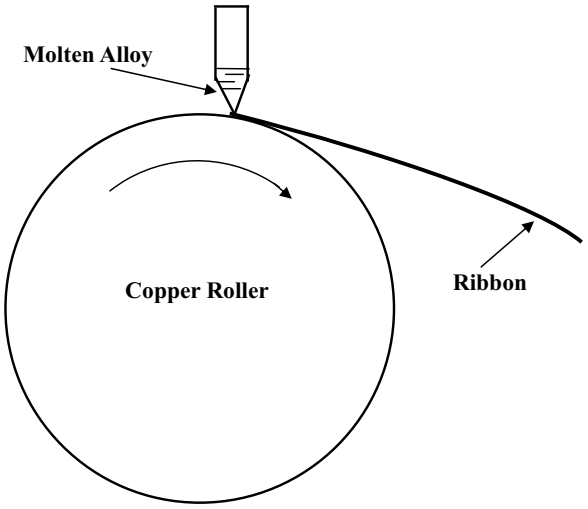

Fig. 1. Schematic of melt-spinning process.

were carried out in an X'Pert PRO MPD diffractometer using Cu Kα1 radiation in a 2θ range from 20° to 90°. The thermal analysis was performed using a Q1000 differential scanning calorimeter with a scanning rate of 5 °C min^{-1} under an Ar protection in a temperature range of 500–700 °C. The microhardness was used to characterize the mechanical property and measured using an HXP-1000M microhardness tester with the applied load of 10 g. Six measurements were performed on one ribbon and the average was reported as the microhardness value.

3. Results and discussion

3.1. Cooling rate and solidification time

The cooling rate and solidification time at the surface of ribbons can be estimated using the following equations proposed by Xu et al. [14]:

$$\left[\frac{\partial T_1}{\partial t}\right]_x = -\frac{b_2(T_{20}-T_{10})x}{2(b_1+b_2)t\sqrt{\pi\alpha_1 t}}\exp\left[-\left(\frac{x}{2\sqrt{\alpha_1 t}}\right)^2\right] \quad (1)$$

$$t_s = \left\{\frac{\sqrt{\pi}x\rho_1[(1-w)L_1 + wL_2 + c_1(T_{10}-T_e)]}{2b_2(T_i - T_{20})}\right\}^2 \quad (2)$$

The definition and values of the parameters for the investigated alloy are listed in Table 2 with an assumption that the alloying elements have no effect on the physical properties of Al–7Si. The solidification time and cooling rate were estimated according to Eqs. (1) and (2) to be 9.13×10^{-6} s and -1.17×10^{7} K s^{-1}, respectively.

In order to simplify the calculation process, the following four assumptions are considered [14]. In particular, (1) the latent heat of crystallization is neglected; (2) there is no gap between the melt-spun ribbon and the cooling copper roller, and then the thermal resistance is neglected. These assumptions may be the reason that the cooling rate estimated using Eqs. (1) and (2) is higher than one of the earlier studies [14]. However, It is also found that the cooling rate of a melt-spun ribbon is between 10^6 and 10^7 K s^{-1} according to the references [15–17]. For example, for 30 μm thick melt-spun ribbon of Al–10.5 wt.% Si, the cooling rate was higher than 10^7 K s^{-1} [15]. The cooling rates are between 10^6 and 10^7 K s^{-1} for Al–Si alloys by melt-spinning [16]. The cooling rate was estimated to be

Table 1
Chemical compositions of A357 alloy investigated (wt.%).

Alloys	Si	Mg	Fe	Ti	Sr (ppm)	Cu, Mn	Al
A357	6.84	0.60	0.10	0.11	0.0011	<0.01	Balance

Table 2
The values of initial conditions and the physical parameters of materials for calculating the cooling rate and solidification time in Eqs. (1) and (2).

Parameter	Materials	
	Al–7Si alloy	Copper roller
Initial temperature, T_0 (°C)	800 (T_{10})	25 (T_{20})
Thermal conductivity, λ (W/(m °C))	168 (λ_1)	398 (λ_2)
Specific heat capacity, c (J/(kg °C))	984 (C_1)	386 (C_2)
Density, ρ (kg/m^3)	2690 (ρ_1)	8930 (ρ_2)
Coefficients of thermal storage, $b=\sqrt{\lambda c\rho}$ (W$\sqrt{\text{s}}$/(m^2 °C))	21087.7 (b_1)	37039.1 (b_2)
Coefficient in Fourier's equation (W m^2/J) $\alpha=\lambda/c,\rho$	0.00006347	–
Latent heat of aluminum crystallization, L_1 (kJ/kg)	396.67	–
Latent heat of silicon crystallization, L_2 (kJ/kg)	1790.02	–
Temperature of the ribbon-roller interface, (°C) $T_i=(b_1T_{10}+b_2T_{20})/(b_1+b_2)$	306.16	–
Eutectic temperature, T_e (°C)	577	–
Distance normal to the roller surface, x (m)	4.6×10^{-5}	–

4.58×10^7 K s^{-1} for 20–40 μm thick melt-spun Al–20 wt.% Si alloy ribbon [17]. The cooling rate was estimated to be about 10^7 K s^{-1} for 36 μm thick melt-spun Al–Si alloy ribbon [9]. Therefore, the estimated cooling rate and solidification time by Eqs. (1) and (2) are valid for the melt-spinning.

3.2. XRD and DSC studies

Fig. 2 shows the XRD patterns of the ingot A357 and the melt-spun ribbons. The XRD pattern of the ingot A357 alloy was present in the peaks of α-Al and Si (Fig. 2a). As illustrated in Fig. 2b, the peaks of primary Si phase totally disappear in the melt-spun ribbon. In other words, the rapid solidification results in an increase in the solubility Si in Al matrix. Moreover, the absence of peaks related to a iron-bearing phase in Fig. 2 may be attributed to the detection limitation of XRD which is typically about 5 vol.% [9].

In addition, it can also seen from Fig. 2 that the measured Al (1 1 1), (2 0 0), (2 1 0) and (2 2 0) peak shifts offer a lattice parameter of about 0.404567 nm. Using the linear relationship between the lattice parameter and the atomic fraction of Si given by Bendjik et al. [16] and assuming nil effect of other alloying elements, a solid solubility of Si in Al matrix of about 2.00 wt.% can be obtained. Considering that the equilibrium solid solubility of Si in Al at room

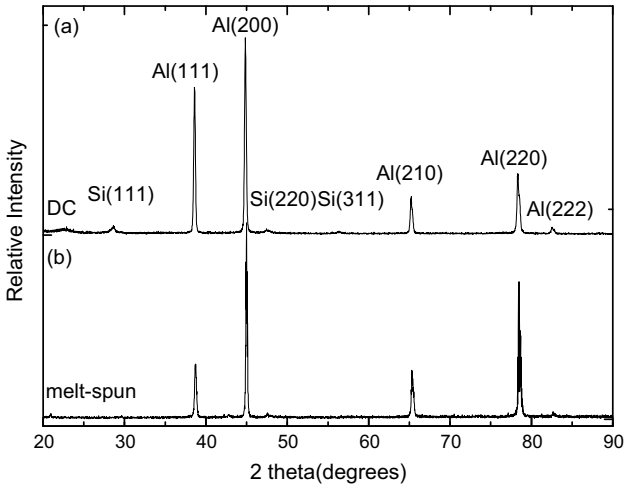

Fig. 2. XRD pattern of samples from DC cast and from the wheel surface of the produced ribbons.

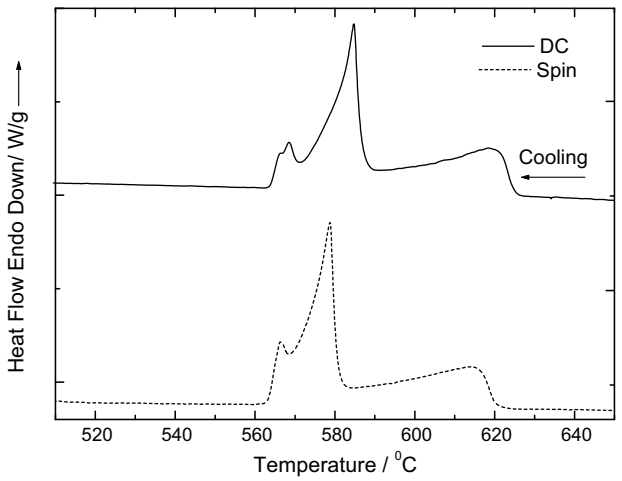

Fig. 3. DSC of melt-spun ribbons and conventional cast sample.

temperature is about 0.05 wt.% [19], the present solid solubility (2.00 wt.%) is much high. As the relationship between the lattice parameter and Si content was just applied for the determination of metastable silicon solid solubility [16], the calculated extension of Si solid solubility is less than the measured value. In addition, it is also found that this extension is lower than those reported in Refs. [12,20] probably because of the lower solidification rate caused by the thicker ribbon (≈46 μm) in this study compared to the reported ribbons (<30 μm)[12,20].

The grain size d was determined using the following equation [21]:

$$d = \frac{K\gamma}{\beta \cos\theta} \tag{3}$$

where the shape factor K is 0.89, the wavelength γ for Cu Kα1 is 1.540598 Å, and the half peak broadening $\beta = (\beta' - 0.05)$. The real half peak broadening β' and the diffraction angle 2θ were measured in Fig. 2. In $\beta = (\beta' - 0.05)$, 0.05 represent the mean value of the XRD instrument error. Thus, the grain size of about 92.0 nm was obtained in this study.

The formation of nanograins is because of the extremely high cooling rate (about 10^7 K s^{-1}). It is well known that constitutional undercooling will result in the solute pileup ahead of the solidification interface. On one hand, solute agents, such as Fe, could act as heterogeneous nucleation sites during the rapid solidification of Al alloys. On the other hand, the solute pileup can be much more pronounced in the case of drastically rapid solidification during melt spinning. Consequently, when the concentration of solute atoms becomes sufficiently high, they may aggregate into small clusters to further enhance the heterogeneous nucleation [22]. Besides, the same mechanism can be dominant in the transformation, precipitation or recrystallization process [23]. Therefore, the formation of nanograins at room temperature is possible.

Another approach to confirm the effect of rapid solidification on the solubility of Si in Al matrix for ribbons produced by melt spinning is the DSC technique. Fig. 3 shows the DSC curve of the melt-spun A357 alloy. It is seen from Fig. 3 that two exothermic peaks shifted to lower temperatures as seen in Table 3. The results imply that α-Al and eutectic Si retained in the super saturated precipitate more readily, and thus they had a higher driving force for precipitation. The 3b peak in the DSC curve in Fig. 3 suggests the precipitation of the Fe-rich π-phase ($Al_8FeMg_3Si_6$). The 3b peak is stronger than the 3a peak for the melt-spun ribbon. The results show that the iron-bearing phase in the melt-spun A357 alloy comprises mostly the script-type π-phase.

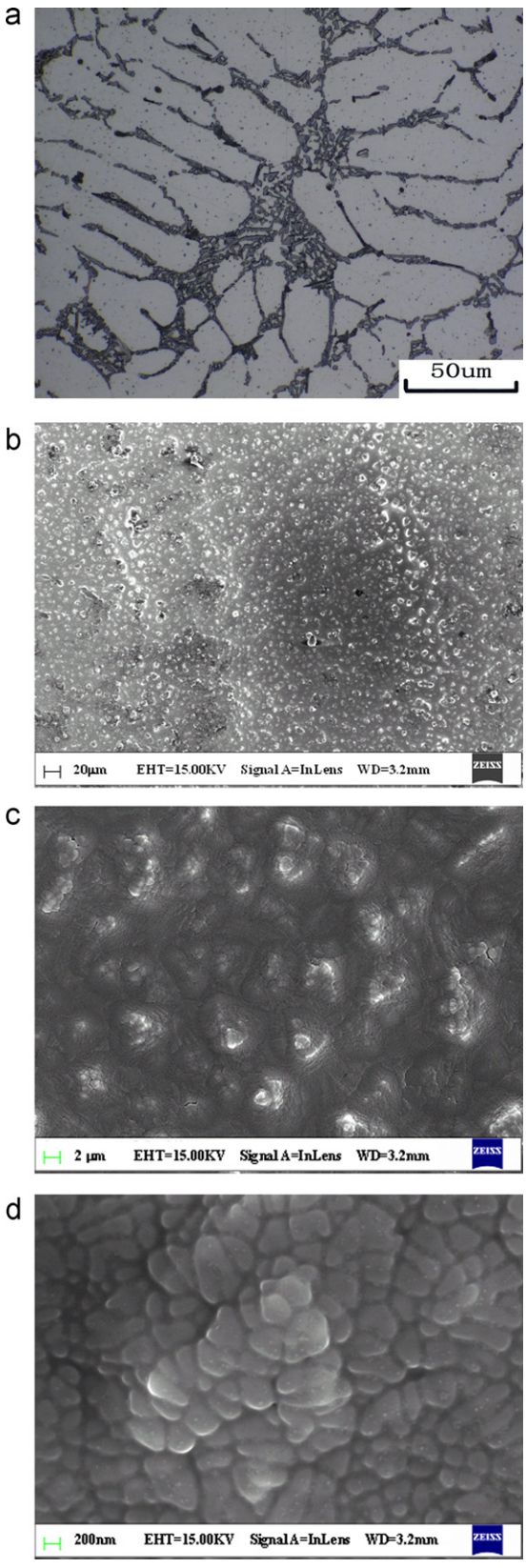

Fig. 4. Microstructure of samples from ingot and the wheel surface of the produced ribbons (a) DC and (b–d) different magnification of melt-spun.

3.3. Microstructure

Fig. 4 shows the optical micrograph of the ingot and the SEM micrograph of the melt-spun A357 ribbons. The ultra-fine and

Table 3
Solidification reactions observed in A357 alloys.

Reaction No.	Reactions [18]	Suggested start temperature [16]/°C	Start to peak temperature in this study/°C	
			DC	Spin
1	L → (α)Al dendrites	611–614	620–626	615–621
2	L → (α)Al + Si	577	585–588	579–580
3a	L → (α)Al + Si + Al_5FeSi	575	568–570	–
3b	L + Al_5FeSi → (α)Al + Si + $Al_8FeMg_3Si_6$	567	566–567	566–568
4	L → (α)Al + Si + Mg_2Si	555	–	–

Table 4
Hardness value of melt-spun ribbons and conventional cast sample.

A357 alloy	Hardness (Vickers) (kg mm^{-2})						Average value
Melt-spun	130	156	141	137	140	143	141.2 ± 7.8
Ingot	77	76	69	65	79	80	74.3 ± 5.5

homogenous dendritic structure is a typical characteristic for the melt-spun ribbons as shown in Fig. 4d. With respect to dendrite arm spacing, its average measured from the SEM micrograph is about 200 nm, while the value of the conventional DC cast alloy is about 17 μm. The eutectic Si crystals are extremely fine in a nano-sized scale of about 50 nm. This is resulted from the rapid solidification by melt spinning.

Meantime, the dendrite arm spacing of the melt-spun ribbon is about 210 nm according to the relationship between the dendrite arm spacing and the cooling rate under the rapid solidification condition for Al alloys [24,25]. Therefore, the result at an extremely high cooling rate is consistent with those reported by other researchers [24,25].

Considering a diffusion path equal to the dendrite arm spacing (λ), the time (t) for homogenizing will be [26]:

$$\lambda^2 = Dt \tag{4}$$

where D is the diffusivity of the element to be homogenized in the Al matrix. As Si is the major alloying element in the present alloy, D can be considered as the diffusivity of Si in Al. Consequently, the ratio of the homogenizing time of the melt-spun ribbon (t_{ms}) to the DC cast one (t_{DC}) will be:

$$\frac{t_{ms}}{t_{DC}} = \frac{\lambda_{ms}^2}{\lambda_{DC}^2} \tag{5}$$

where λ_{ms} and λ_{DC} are the dendrite arm spacings of the melt-spun and DC cast samples, respectively. Substituting the values of λ_{ms} (about 200 nm) and λ_{DC} (about 17 μm) into Eq. (5), the value of t_{ms}/t_{DC} is about 0.000138, which means that the time for homogenizing a melt-spun nanostructure is about 7000 times shorter than that for the DC cast sample. This can save the homogenizing treatment for the melt-spun ribbon.

3.4. Microhardness

The Vickers microhardness of the melt-spun and DC cast samples is summarized in Table 4. It is clear that the microhardness of the nanostructured melt-spun ribbon is twice as much as that of the DC cast one. It is also found that the microhardness of the melt-spun A357 is similar to the reported value of the melt-spun Al–7.6 wt.% Si alloy (146 kg mm^{-2}) [27] and lower than that of the melt-spun Al–12 wt.% Si (224 kg mm^{-2}) [9] and Al–20 wt.% Si (182 kg mm^{-2}) [20]. The high microhardness of the melt-spun alloy compared to its DC ingot could be attributed to the presence of the nanostructure as well as super saturated Si in Al matrix. The lower hardness in this study than the reported ones [9,20] could be resulted from lower Si content in Al–Si alloys.

4. Conclusions

(1) The solidification time and cooling rate of 46 μm thick melt-spun A357 alloy ribbon were estimated to be 9.13×10^{-6} s and 1.17×10^7 K s^{-1}, respectively.
(2) The rapid solidification in this study has a significant influence on the phase of A357 alloy extending the solid solubility of Si in Al matrix to 2.00 wt.%. In comparison with the DC alloy, primary Si was not observed in the melt-spun ribbon. DSC results further confirm this conclusion and the iron-bearing phase in melt-spun ribbon comprises mostly the script-type π-phases.
(3) The ultra-fine and homogenous dendritic structure was observed in the melt-spun ribbon. The dendrite arm spacing reduced to about 200 nm compared to about 17 μm in the DC cast alloy. The nano-sized spherical eutectic Si having a size of 50 nm was formed by melt spinning and the grain size of the melt-spun ribbon was about 92 nm.
(4) The microhardness of the melt-spun A357 alloy is twice as high as that of the DC cast ingot.

Acknowledgements

The project was supported by Research Fund of the State Key Laboratory of Solidification Processing (NO.42-QP-009), Fundamental Research Fund of Northwestern Polytechnical University (NO. JC200929) and the 111 Project (NO. B08040). Authors also thank Dr. Richard Thackray at the University of Sheffield in UK for this study.

References

[1] M. Rajabi, M. Vahidi, A. Simchi, P. Davami, Mater. Charact. 60 (2009) 1370–1381.
[2] R. Trivedi, F. Jin, I.E. Anderson, Acta Mater. 51 (2003) 289–300.
[3] O. Uzun, T. Karaaslan, M. Gogebakan, M. Keskin, J. Alloys Compd. 376 (2002) 149–157.
[4] R.M. Shalaby, J. Alloys Compd. 505 (2010) 113–117.
[5] Y.E. Kalay, L.S. Chumbley, I.E. Anderson, R.E. Napolitano, Metall. Mater. Trans. A 38 (2007) 1452–1457.
[6] Y. Birol, J. Alloys Compd. 439 (2007) 81–86.
[7] A.K. Srivastava, V.C. Srivastava, A. Gloter, S.N. Ojha, Acta Mater. 54 (2006) 1741–1748.
[8] E. Karaköse, M. Keskin, J. Alloys Compd. 479 (2009) 230–236.
[9] M. Salehi, K. Dehghani, J. Alloys Compd. 457 (2008) 357–361.
[10] K. Dehghani, M. Salehi, M. Salehi, H. Aboutalebi, Mater. Sci. Eng. A 489 (2008) 245–252.
[11] C. Triveño Rios, M.M. Peres, C. Bolfarini, W.J. Botta, C.S. Kiminami, J. Alloys Compd. 495 (2010) 386–390.
[12] Y. Birol, J. Mater. Sci. 31 (1996) 2139–2143.
[13] O. Uzun, F. Yılmaz, U. Kolemen, N. Başman, J. Alloys Compd. 509 (2011) 21–26.
[14] C.L. Xu, H.Y. Wang, F. Qiu, Y.F. Yang, Q.C. Jiang, Mater. Sci. Eng. A 417 (2006) 275–280.
[15] B.G. Lewis, I.W. Donald, H.A. Davies, Proceedings of an International Conference on Solidification, The University of Sheffield, UK, July, 1977.
[16] A. Bendjik, R. Delhez, L. Katgerman, Th. De Keijser, E.J. Mittemeijer, N.M. Van Der Pers, J. Mater. Sci. 15 (1980) 2803–2810.
[17] M. Rajabi, A. Simchi, P. Davami, Mater. Sci. Eng. A 492 (2008) 443–449.
[18] L. Bäckerud, G. Chai, J. Tamminen, Solidification of Aluminum Alloys. AFS/SKAN-Aluminum, vol. 2, American Foundrymen's Society (AFS), Des Plaines, IL, USA, 1990, pp. 128–150.
[19] E.M. Ahmed, Mater. Lett. 62 (2008) 960–963.
[20] M. Van Rooyen, N.M. Van Der Pers, Th.H. de Keijser, E.J. Mittemeijer, Mater. Sci. Eng. 96 (1987) 17–25.

[21] B.D. Cullity, Elements of X-Ray Diffraction, vol. 1, Addison-Wesley Pub. Co., 2003.
[22] B. Cantor, K. O'Reilly, Solifification and Casting, Institute of Physics Publishing, London, UK, 2003, pp. 199–247.
[23] M. Ferry, Direct Strip Casting of Metals and Alloys, Woodhead Publishing Limited, Cambridge, England, 2006, pp. 214–230.
[24] M.C. Flemings, T.Z. Kattamis, B.P. Bardes, AFS Trans. 99 (1991) 501–506.
[25] P.N. Crepeau, W.T. Whited, M.E. Hoover, AFS Trans. 105 (1997) 775–781.
[26] R.E. Reed-hill, R. Abbaschian, Physical Metallurgy Principles, PWSKENT Publishing Co., 1992, pp. 444–467.
[27] S.K. Bose, R. Kumar, J. Mater. Sci. 8 (1973) 1795–1799.